

Tadpole shaped $\text{Ge}_{0.96}\text{Mn}_{0.04}$ magnetic semiconductors grown on Si

Yong Wang,¹ Faxian Xiu,² Jin Zou,^{1,3,a)} Kang L. Wang,^{2,a)} and Ajey P. Jacob⁴

¹Materials Engineering, The University of Queensland, Brisbane QLD 4072, Australia

²Department of Electrical Engineering, University of California at Los Angeles, California 90095, USA

³Centre for Microscopy and Microanalysis, The University of Queensland, Brisbane QLD 4072, Australia

⁴Technology and Manufacturing Group External Programs, Intel Corporation, Santa Clara, California 95052, USA

(Received 22 September 2009; accepted 29 December 2009; published online 3 February 2010)

Magnetic and structural properties of a $\text{Ge}_{0.96}\text{Mn}_{0.04}$ thin film grown on Si has been investigated by transmission electron microscopy and superconducting quantum interference device. Tadpole shaped coherent GeMn clusters induced by spinodal decomposition were revealed in the film. Although these coherent clusters are dominant, Mn_5Ge_3 precipitates can be still detectable, contributing to a complex ferromagnetism. The Ge buffer layer, by relieving the misfit strain between Si and Ge, can significantly reduce the density of lattice defects in the subsequent GeMn layer. Our findings unveil a particular morphology of GeMn clusters, which would contribute to better understand the GeMn system. © 2010 American Institute of Physics.

[doi:10.1063/1.3297880]

The Ge/Si heterostructure, taking advantage of the band offset between Si and Ge, has been widely used in today's complementary metal-oxide-semiconductor technology. The resultant two dimensional carrier gas may enhance their mobilities and therefore device performance.¹ For this reason, Ge-based (such as GeMn) diluted magnetic semiconductors (DMSs), compatible with the current Si technology, have been studied extensively.^{2–13} It is well understood that the low solubility of Mn in Ge has been a main barrier to achieve a high T_c DMS GeMn film with high Mn concentration and uniformly distributed Mn in Ge. As a consequence, Mn-rich precipitates, such as Mn_5Ge_3 ,^{9,14,15} Mn_5Ge_2 , and $\text{Mn}_{11}\text{Ge}_8$,¹² are usually observed and are believed to be responsible for the observed ferromagnetism up to room temperature. Apart from these precipitates, Jamet *et al.*⁵ has reported self-organized GeMn nanocolumns with over 400 K ferromagnetism. The similar self-assembled nanostructures were also observed by other groups in Mn-doped Ge thin films prepared by molecular beam epitaxy (MBE).^{8,12} On the other hand, randomly distributed coherent GeMn nanodots with a nonuniform size have been grown on Ge substrates using MBE;⁷ however, no spontaneous magnetization was observed at all temperatures (down to 2 K). This indicates that different morphologies (nanocolumns/nanodots) of the GeMn clusters may result in different magnetic properties. Indeed, it has been reported that the distribution of Mn atoms, which depends strongly upon the substrate temperature and the Mn concentration, can critically affect their charge state and magnetic coupling.^{8,9} For this reason, it is essential to further explore the nature of different morphology of the GeMn clusters to have a better understanding of the structure-property relationship of the GeMn system.

In this letter, by employing detailed transmission electron microscopy (TEM), energy dispersive spectroscopy (EDS) in the scanning TEM (STEM) mode and superconducting quantum interference device (SQUID) investigations, the magnetic and structural properties of the $\text{Ge}_{0.96}\text{Mn}_{0.04}$ thin

film grown on Si (001) substrates with a Ge buffer layer are comprehensively investigated.

The $\text{Ge}_{0.96}\text{Mn}_{0.04}$ thin films were grown on Si (001) substrates by a Perkin–Elmer solid source MBE with nominal thickness of 85 nm. The Si substrates were cleaned by $\text{H}_2\text{SO}_4:\text{H}_2\text{O}_2$ (5:3) and 10% HF with a final step of HF etching. Native oxide was removed by 800 °C annealing for 10 min in vacuum. First, a Ge buffer layer of 35 nm was deposited at 400 °C. After that, 4% Mn-doped Ge was deposited with a growth rate of 0.02 nm/s on Si (001) substrate at 70 °C. The nanostructure and compositional variations of the samples was characterized by cross-sectional TEM and EDS in a FEI Tecnai F20 TEM. TEM specimens were prepared using a tripod technique, followed by a final thinning using a Gatan precision ion polishing system.

Figures 1(a) is a typical cross-sectional TEM image and shows the general morphology of the GeMn thin film. From this figure, nanoscaled tadpoles with dark contrast can be clearly seen on the top part of the thin film with one marked as an example. The inset is a selected area electron diffrac-

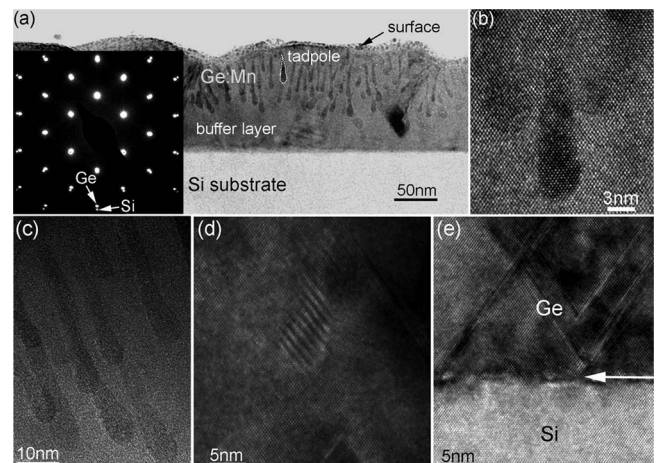


FIG. 1. (a) A low magnification TEM image showing GeMn tadpoles and the inset shows the SAED pattern; (b) a HRTEM image of typical GeMn tadpoles; (c) tadpoles from another direction; (d) a precipitate formed within the film; (e) the interface between Ge buffer layer and Si.

^{a)}Authors to whom correspondence should be addressed. Electronic addresses: j.zou@uq.edu.au and wang@ee.ucla.edu.

tion pattern (SAED) taken along a $\langle 110 \rangle$ direction including the GeMn film and the Si substrate. This SAED pattern can be indexed by the diamond structured Ge and Si, indicating a relaxed Ge layer grown on Si. In order to understand the structure of the tadpoles, high resolution TEM experiments were carried out and the result is shown in Fig. 1(b). Careful examination of the high resolution TEM (HRTEM) image verifies that the GeMn tadpoles have the same diamond structure as the Ge matrix, indicating a coherent growth.^{5,7} The dark contrast of the GeMn clusters is caused by the local strain, which is induced by the larger Mn atoms incorporated into rigid Ge lattice as the atomic radius of Mn (140 pm) is larger than that of Ge (125 pm).¹⁶ In fact, similar phenomena have been observed in GeMn nanocolumns⁵ and GeMn nanodots.⁷ To further clarify the morphology and structure of tadpoles, the TEM specimen was tilted along the axial direction of the tadpoles and a typical result is shown in Fig. 1(c), in which the tadpoles are indeed coherent clusters, rather than secondary precipitates. In order to confirm other possible precipitations, extensive TEM investigations were carried out and, very occasionally, small particles can be identified. Figure 1(d) shows such an example where moiré fringes can be observed in the middle of Fig. 1(d), indicating the existence of other precipitates. Since there is $\sim 4\%$ lattice mismatch between Ge and Si, it is necessary to evaluate their interface as the interface quality may be directly related to the property of the system. Figure 1(e) is a typical HRTEM image of the interface between the Ge buffer layer and the Si substrate, and shows a well epitaxial relationship, although a high density of lattice defects (mostly in the form of stacking faults) can be observed above the interface, result in a rough surface of the finally grown film, as shown in Fig. 1(a). Although we cannot distinguish the interface between the Ge buffer layer and the GeMn layer (due to their almost no lattice mismatch), the fact that a very low density of lattice defects can be found in the GeMn layer [comparing Figs. 1(b) and 1(c) with Fig. 1(e)] suggests that the lattice defects are mainly located in the Ge buffer layer. Indeed, one can observe some stacking faults crossing each other right from the interface of Si/Ge buffer layer [Fig. 1(e)], which may lead to the interaction between defects and significantly decrease the defect density in the subsequent GeMn layer. Therefore, it is critical to grow the buffer layer to eliminate the possible lattice defects in the GeMn layer. It should be noted that the Ge buffer layer is defective, which may not benefit the carrier transport. However, based on our previous studies,^{17,18} high quality Ge on Si with low threading dislocation density of $\sim 10^4 \text{ cm}^{-2}$ may be achieved through Sb surfactants and/or graded SiGe buffer layers. By employing these established techniques, it is anticipated that high quality GeMn grown on Si with low density of defects may be achievable.

In order to understand the composition of the dark tadpoles, EDS experiments in the STEM mode were carried out on the cross-sectional TEM specimens and a typical STEM image is shown in Fig. 2(a). It should be noted that the tadpoles appear dark contrast in the TEM mode (Fig. 1) which is different from the case in the STEM mode [Fig. 2(a)] where the tadpoles show white contrast. The EDS result is shown in Fig. 2(b) where the Mn and Ge peaks are clearly seen. Figure 2(c) presents the result of the line scanning using the Mn K peak for the tadpoles in the STEM image [Fig.

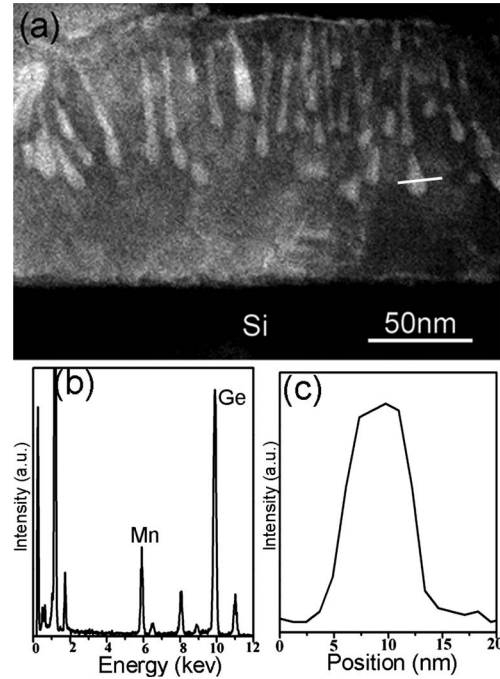


FIG. 2. (a) A STEM cross-sectional image showing GeMn tadpoles (white contrast); (b) A EDS profile taken from a tadpole showing strong Mn and Ge peaks; (c) a line scan profile of the marked line in (a) using the Mn K peak, confirming the white spots are Mn-rich areas.

2(a)], clearly indicating that Mn is rich inside the tadpoles. Extensive quantitative EDS measurements show that the Mn concentration could be up to 17% inside the tadpoles.

A SQUID magnetometer was used to obtain temperature-dependent hysteresis loops and magnetization moments in zero-field cooled (ZFC) and field cooled (FC) processes, as shown in Figs. 3(a) and 3(b), respectively. The GeMn tadpoles exhibit a saturation moment of 25 kA/m (at 10 K) compared with the reported value of $\sim 8 \text{ kA/m}$ for $\text{Ge}_{0.98}\text{Mn}_{0.02}$.² The saturation moments per Mn atom can be estimated to be $0.9 \mu_B$. Provided that each Mn has a theoretical moment of $3 \mu_B$,¹⁹⁻²¹ this gives a fraction of roughly 30% of Mn being activated in the GeMn layer.

The ZFC curve was obtained by cooling the sample under zero magnetic field from 350 to 10 K, and subsequently measuring the magnetic moments while the sample was warmed up under a field of 200 Oe. For the FC process, however, the sample is cooled through its Curie temperature (T_c) in the presence of a magnetic field (200 Oe). The difference between these two processes gives an insight of phase transformation, the blocking temperature (T_b), and T_c . Based on the temperature dependent hysteresis loops and ZFC and FC curves shown in Fig. 3, the GeMn tadpoles show several

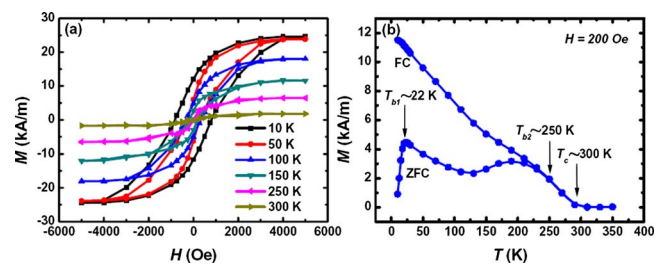


FIG. 3. (Color online) SQUID measurements of a 4% Mn-doped Ge thin film grown on Si substrate. (a) hysteresis loops measured at different temperatures; (b) ZFC and FC curves measured with a magnetic field of 200 Oe.

features as elaborated in the following: (a) The magnetic moment decreases to zero when the temperature reaches room temperature, which indicates a T_c of ~ 300 K. The origin of room temperature T_c is associated with the precipitate of Mn_5Ge_3 .^{15,22} As mentioned above, we occasionally found precipitates in our extensive TEM investigations. It is believed that these precipitates are most likely the Mn_5Ge_3 phase. (b) Coercivity values decrease to zero when the temperature approaches 250 K [Fig. 3(a)], in a good agreement with the results from the ZFC and FC curves [Fig. 3(b)]. This indicates a T_b of about 250 K ($T_{b2} \sim 250$ K). The T_b origin has been attributed to the formation of Mn_5Ge_3 in GeMn.^{3,15} When $250 \text{ K} < T < 300 \text{ K}$, the precipitates are expected to react freely on an externally applied magnetic field like a superparamagnet.¹⁵ So this temperature region corresponds to a superparamagnetic regime. (c) The ZFC curve shows another T_b of ~ 22 K ($T_{b1} \sim 22$ K). In recent years, there have been wide debates on the origin of the ferromagnetism in GeMn.^{2,3,23,24} In 2002, Park *et al.*² reported a T_c of 116 K from a $\text{Ge}_{1-x}\text{Mn}_x$ thin film with a Mn concentration of 3.5%. The switching of the ferromagnetic ordering in a gated Hall bar sample demonstrated that the ferromagnetism was hole-mediated. In contrast, Li *et al.*³ observed two different ordering temperatures T_c and T_c^* ($T_c < T_c^*$) in the secondary-phase free $\text{Ge}_{1-x}\text{Mn}_x$ thin films. A T_c of 12 K ($x=0.05$) was attributed to the global ferromagnetic ordering while T_c^* of 120 K presented the onset of local ferromagnetism associated with isolated spin clusters, indicating that the $\text{Ge}_{1-x}\text{Mn}_x$ is far away from being a high- T_c DMS. Jaeger *et al.*,²⁴ however, showed extensive experimental evidence that the GeMn exhibits a spin-glasslike behavior with two transition temperatures $T_f=12$ K and $T_b=250$ K. Their origins were attributed to the blocking or freezing transitions of two different kinds of superparamagnetic precipitates. Similarly, Ahlers *et al.*¹⁵ provided a detailed analysis on magnetic behaviors of the Mn_5Ge_3 precipitates and lattice-coherent nanoclusters, which explained the blocking temperatures at 250 and 12 K, respectively. Likewise, we also observed two transition temperatures at $T_{b1} \sim 22$ K (nanoclusters) and $T_{b2} \sim 250$ K (Mn_5Ge_3) as shown in the ZFC process [Fig. 3(b)]. When decreasing temperatures below T_{b1} , the magnetization decreases as a result of nanocluster freezing; while for increasing temperatures above T_{b2} , the magnetization decreases due to the thermal energy exceeding nanocluster interactions [Fig. 3(b)].²⁴ Same analysis can be applied to the Mn_5Ge_3 precipitates which have a transition temperature of ~ 250 K [Fig. 3(b)]. These magnetic behaviors are also consistent with many other magnetic semiconductor systems, such as Mn doped GaN (Ref. 25) and Te-doped MnGaAs.²⁶

It is of interest to explore how the coherent GeMn tadpoles were formed during the GeMn epitaxially grown on Si with a Ge buffer layer. It has been reported that coherent growth can be achieved by spinodal decomposition in magnetic impurities doped semiconductors, such as (Ga,Mn)As, (Ga,Mn)N, and (Zn,Cr)Te magnetic semiconductors.²⁷ For example, Mn-rich GaAs quantum-dotlike nanocrystals can be embedded within a Mn-poor matrix, while maintaining the same crystal structure as the matrix.^{27,25} Indeed, many studies have shown the evidence of the spinodal decomposition in their magnetic semiconductors, such as (Ga,Mn)As (Ref. 28) and (Zn,Cr)Te,²⁷ indicating that the spinodal decomposition (resulting in dopant-rich nanocrystals) is a com-

mon phenomenon in such a hybrid system when the concentration of magnetic dopants is appropriate. In general, if the GeMn film grown on a substrate with a relatively low temperature, Mn-rich coherent GeMn nanocolumns^{5,8} and nanodots⁷ would be main clusters; while the Mn-rich secondary phases such as Ge_3Mn_5 (Refs. 9, 14, and 15) and $\text{Ge}_8\text{Mn}_{11}$ (Ref. 12) become dominant if the GeMn film is grown at a relatively high temperature. This indicates that the nature and the morphology of the resultant Mn-rich clusters are highly dependent on the growth parameters, such as growth temperature, the growth rate, and the Mn concentration. For our case, when the Mn content reaches a critical point at a certain thickness of several nanometers (estimated value from the growth conditions), coherent Mn-rich clusters start to grow and attract the surrounding Mn during the codeposition of Ge and Mn, leading to a Mn poor region in the adjacent areas. As the Mn-rich cluster continues growing and becomes larger (need to capture more Mn), no sufficient Mn would be available in the adjacent areas. This makes the Mn-rich area gradually become smaller and smaller far from the nucleation centers during the growth, which eventually results in the formation of a tadpole shaped Mn-rich area.

In conclusion, we have fabricated tadpole shaped GeMn dominated magnetic semiconductors thin films. The complicated ferromagnetism found in the film can be well explained by co-contribution of coherent GeMn tadpoles and Mn_5Ge_3 precipitates. The formation of such GeMn tadpoles involves spinodal decomposition and inhomogeneous Mn diffusion. As Si acts as the substrate, stacking faults induced by the large lattice mismatch make the thin film surface rough and the tadpoles misaligned along the growth direction.

The Australia Research Council, the Focus Center Research Program-Center on Functional Engineered Nano Architectonics, Western Institution of Nanoelectronics and Intel (Spin-Gain FET project) (UCLA) are acknowledged for their financial support of this project.

¹K. L. Wang *et al.*, *J. Mater. Sci.: Mater. Electron.* **6**, 311 (1995).

²Y. D. Park *et al.*, *Science* **295**, 651 (2002).

³A. P. Li *et al.*, *Phys. Rev. B* **72**, 195205 (2005).

⁴M. I. van der Meulen *et al.*, *Nano Lett.* **9**, 50 (2009).

⁵M. Jamet *et al.*, *Nature Mater.* **5**, 653 (2006).

⁶C. Bihler *et al.*, *Appl. Phys. Lett.* **88**, 112506 (2006).

⁷D. Bougeard *et al.*, *Phys. Rev. Lett.* **97**, 237202 (2006).

⁸A. P. Li *et al.*, *Phys. Rev. B* **75**, 201201 (2007).

⁹Y. Wang *et al.*, *J. Appl. Phys.* **103**, 066104 (2008).

¹⁰Y. X. Chen *et al.*, *Appl. Phys. Lett.* **90**, 052508 (2007).

¹¹P. De Padova *et al.*, *Surf. Sci.* **601**, 2628 (2007).

¹²Y. Wang *et al.*, *Appl. Phys. Lett.* **92**, 101913 (2008).

¹³Y. M. Cho *et al.*, *J. Magn. Magn. Mater.* **282**, 385 (2004).

¹⁴L. Ottaviano *et al.*, *Appl. Phys. Lett.* **88**, 061907 (2006).

¹⁵S. Ahlers *et al.*, *Phys. Rev. B* **74**, 214411 (2006).

¹⁶J. C. Slater, *J. Chem. Phys.* **41**, 3199 (1964).

¹⁷J. L. Liu *et al.*, *J. Appl. Phys.* **99**, 024504 (2006).

¹⁸J. L. Liu *et al.*, *Appl. Phys. Lett.* **75**, 1586 (1999).

¹⁹A. Stroppa *et al.*, *Phys. Rev. B* **68**, 155203 (2003).

²⁰T. C. Schulthess and W. H. Butler, *J. Appl. Phys.* **89**, 7021 (2001).

²¹M. V. Schilfgaarde and O. N. Mryasov, *Phys. Rev. B* **63**, 233205 (2001).

²²A. Verna *et al.*, *Phys. Rev. B* **74**, 085204 (2006).

²³H. Liet *et al.*, *J. Appl. Phys.* **100**, 103908 (2006).

²⁴C. Jaeger *et al.*, *Phys. Rev. B* **74**, 045330 (2006).

²⁵S. Dhar *et al.*, *Phys. Rev. B* **67**, 165205 (2003).

²⁶S. U. Yuldashev *et al.*, *Phys. Rev. B* **70**, 193203 (2004).

²⁷T. Dietl, *Nature Mater.* **5**, 673 (2006).

²⁸W. Z. Wang *et al.*, *Appl. Phys. Lett.* **91**, 202503 (2007).